J. Math. Biol. (2010) 61:649–663
DOI 10.1007/s00285-009-0315-2

Mathematical Biology

A Lagrangian particle method for reaction–diffusion systems on deforming surfaces

Michael Bergdorf · Ivo F. Sbalzarini · Petros Koumoutsakos

Received: 18 February 2009 / Revised: 28 October 2009 / Published online: 18 December 2009

Abstract Reaction–diffusion processes on complex deforming surfaces are fundamental to a number of biological processes ranging from embryonic development to cancer tumor growth and angiogenesis. The simulation of these processes using continuum reaction–diffusion models requires computational methods capable of accurately tracking the geometric deformations and discretizing on them the governing equations. We employ a Lagrangian level-set formulation to capture the deformation of the geometry and use an embedding formulation and an adaptive particle method to discretize both the level-set equations and the corresponding reaction–diffusion. We validate the proposed method and discuss its advantages and drawbacks through simulations of reaction–diffusion equations on complex and deforming geometries.

Mathematics Subject Classification (2000) 92C15 · 35Q92 · 76M28

1 Introduction

In the seminal work of D'Arcy Thompson on Growth and Form Thompson (1942), spatially dependent chemical reactions and diffusive processes have been postulated as key mechanisms that determine the growth and structural characteristics of several organisms. Turing (1952) proposed reaction–diffusion models that depend on local autocatalysis and long-range inhibition to explain a wide range of biological pattern formation phenomena Murray (2002).

M. Bergdorf · P. Koumoutsakos (✉)
Department of Computational Science, ETH Zurich, Zurich, Switzerland
e-mail: petros@ethz.ch

I. F. Sbalzarini
Institute of Theoretical Computer Science and Swiss Institute of Bioinformatics,
ETH Zurich, Zurich, Switzerland

The role of the surface geometry on pattern formation as described by reaction–diffusion processes has attracted in the recent years significant attention as several biological pattern forming processes take place on complex deforming geometries. Koch and Meinhardt (1994) reviewed the generation of stripe and spot patterns by activator-inhibitor and activator-substrate systems. Varea et al. (1999) considered a linearized Brusselator system on a sphere. Chaplain et al. (2001) considered the Schnakenberg system on a sphere, suggesting that pre-pattern formation conditions may play a role in solid tumor growth through the distribution of growth-promoting factors on the tumor boundary. The effect of spatial extension on reaction–diffusion patterns was thoroughly investigated by Baker and Maini (2007), and Madzvamuse and Maini (2007). The two-way coupling of space and patterning was investigated by Harrison and Kolar (1998) and Holloway and Harrison (1999) in a computational study of algal growth. These simulations were later extended to three space dimensions Harrison et al. (2001), employing a triangulated representation of the geometry. The nodes of this triangulation are moved according to the local concentration of a morphogen in order to simulate growth processes. A similar approach was used to study the growth of corals through diffusion-limited aggregation Kaandorp et al. (2005). Surface triangulations enable computations using suitable finite element approximations Bänsch et al. (2005), but they may become computationally intensive if this triangulation needs to be repeated, as is the case on growing and deforming surfaces. An effective way of representing complex deforming surfaces is by the implementation of level sets. Bertalmio et al introduced a method to perform diffusion calculations on surfaces that are represented by level sets in three dimensions Bertalmio et al. (2001). The original data lying on the surface are extended to a thin band around the interface and the differential operators are adapted accordingly, so that all the computations are performed on a fixed Cartesian grid, corresponding to a function embedding of the actual surface by level sets. Although the method was developed for application to computer graphics problems, the authors also presented two examples of reaction–diffusion patterns on complex implicit surfaces. Xu and Zhao (2003) and Adalsteinsson and Sethian (2003) independently proposed a level-set method for the transport of surface-bound substances on a deforming interface. Both works employed a non-conservative formulation based on level-set interface capturing and showed results of passive convection of an interface with an associated surfactant. Level sets coupled to reaction–diffusion systems have recently also been applied to the study of solid tumor growth Macklin et al. (2009). Some accuracy and robustness aspects of this type of embedding methods have recently been addressed for the simple closest-point variant Ruuth and Merriman (2008).

Level-set formulations largely rely on Eulerian formulations of the governing equations, while additional randomly seeded marker particles can be introduced to improve the capturing of the interface Enright et al. (2002). The level-set equations are hyperbolic and as such they are well suited to a Lagrangian formulation. A particle method that discretizes the Lagrangian formulation of the level-set equations was introduced in Hieber and Koumoutsakos (2005). One key feature of this Lagrangian particle formulation is that rigid-body rotations and translations are treated with very high accuracy (errors only due to initialization and time stepping), as there is no distortion of the computational elements. In cases where the particle locations get distorted by the flow map,

a remeshing procedure is introduced to regularize the particle locations. This method has been enhanced by wavelet-based multiresolution capabilities, leading to simulations of unprecedented accuracy and efficiency Bergdorf and Koumoutsakos (2006).

In the present work we extend the formulation presented in Hieber and Koumoutsakos (2005) and combine it with the techniques introduced by Bertalmio et al Bertalmio et al. (2001) to develop a novel adaptive particle method that is capable of efficient simulations of reaction–diffusion processes on complex and deforming surfaces. The method maintains the Lagrangian adaptivity of particle methods and demonstrates that the proposed particle framework can handle the solution of partial differential equations evolving not only in the lumen, but also on the surface of three-dimensional deforming geometries. The capabilities of the method are demonstrated on a number of benchmark problems and its advantages and drawbacks are discussed.

The article is structured as follows: in Sect. 2 we derive the governing equations. Section 3 is devoted to the presentation of the particle method and Sect. 4 presents results of pattern-forming reaction–diffusion systems on geometries deforming according to the local concentration of a surface chemical component. Section 5 will summarize the strengths and limitations of the presented approach.

2 Reaction–diffusion systems on general geometries

We consider reaction–diffusion equations on a closed smooth surface $\Gamma \subset \Omega \subseteq \mathbb{R}^3$. A general reaction–diffusion system for N_S species on Γ can be written as:

$$\frac{\partial c_s}{\partial t} = F_s(c_1, c_2, \ldots, c_s) + \nabla_\Gamma \cdot \left(\underline{\underline{\boldsymbol{D}}}_s \nabla_\Gamma c_s \right), \tag{1}$$

where $s = 1, 2, \ldots, N_S$; F_s represents the reaction terms for species s and $\underline{\underline{\boldsymbol{D}}}_s$ denotes the diffusion tensor associated with species s. For simplicity of presentation in the following we will only consider homogeneous isotropic diffusion, i.e.

$$\underline{\underline{\boldsymbol{D}}}_s = D_s \mathbb{1}, \qquad s = 1, 2, \ldots, N_S, \tag{2}$$

where D_s is a scalar constant. Equation (1) then simplifies to

$$\frac{\partial c_s}{\partial t} = F_s(c_1, c_2, \ldots, c_s) + D_s \Delta_\Gamma c_s. \tag{3}$$

The operator Δ_Γ is called the Laplace–Beltrami operator on Γ.

We now consider a geometry that changes in time, i.e.

$$\Gamma(t) = \{\boldsymbol{x}_\Gamma(t)\}, \tag{4}$$

with

$$\frac{d\boldsymbol{x}_\Gamma}{dt} = \boldsymbol{u}(\boldsymbol{x}_\Gamma, \boldsymbol{c}, \Gamma), \tag{5}$$

where $\boldsymbol{u}$ is a velocity in $\mathbb{R}^d$ defined on Γ.

Together with Eq. (5) the governing equations of the full system are then given by

$$\frac{\partial c_s}{\partial t} + \nabla_\Gamma \cdot (c_s \, \boldsymbol{u}) = F_s(\boldsymbol{c}) + D_s \, \Delta_\Gamma c_s . \tag{6}$$

Using the surface normal $\boldsymbol{n}$, Eq. (6) can be rewritten as

$$\frac{\partial c_s}{\partial t} + ((\mathbb{1} - \boldsymbol{n} \otimes \boldsymbol{n}) \cdot \nabla) \, (c_s \, \boldsymbol{u}) = F_s(\boldsymbol{c}) + D_s \nabla \cdot ((\mathbb{1} - \boldsymbol{n} \otimes \boldsymbol{n}) \nabla c_s), \tag{7}$$

see Stone (1990) for details of the derivation. In order to solve this problem with particle methods, it is more suitable to write Eq. (7) as a conservation law:

$$\begin{aligned} \frac{\partial c_s}{\partial t} + \nabla \cdot (c_s \, \boldsymbol{u}) = (\boldsymbol{u} \cdot \boldsymbol{n}) \frac{\partial c_s}{\partial n} + c_s \, \boldsymbol{n} \cdot (\boldsymbol{n} \cdot \nabla) \boldsymbol{u} \\ + F_s(\boldsymbol{c}) + D_s \nabla \cdot ((\mathbb{1} - \boldsymbol{n} \otimes \boldsymbol{n}) \nabla c_s) \, . \end{aligned} \tag{8}$$

The reformulation from (7) to (8) involves the telescopic expansion

$$\nabla_\Gamma = (\mathbb{1} - \boldsymbol{n} \otimes \boldsymbol{n}) \nabla = \nabla - \boldsymbol{n} \otimes \boldsymbol{n} \nabla .$$

Even though the operator has only components in Γ, the separate application of the Ω-space operators ∇ and $\boldsymbol{n} \otimes \boldsymbol{n} \nabla$ necessitates the extension of both c_s and $\boldsymbol{u}$ from Γ to Ω. The only requirement on this extension is that it is differentiable. Inspecting the first two terms on the right-hand side of Eq. (8), however, we realize that if we extend c_s and $\boldsymbol{u}$ such that

$$\frac{\partial c_s}{\partial \boldsymbol{n}} = 0 \quad \text{and} \quad \frac{\partial (\boldsymbol{n} \cdot \boldsymbol{u})}{\partial \boldsymbol{n}} = 0 \, , \tag{9}$$

we can simplify Eq. (8) to

$$\frac{\partial c_s}{\partial t} + \nabla \cdot (c_s \, \boldsymbol{u}) = F_s(\boldsymbol{c}) + D_s \nabla \cdot ((\mathbb{1} - \boldsymbol{n} \otimes \boldsymbol{n}) \nabla c_s) \, . \tag{10}$$

In the present work, the surface Γ is represented implicitly by the zero iso-surface of a level-set function $\varphi(\boldsymbol{x})$, thus:

$$\Gamma = \{ \, \boldsymbol{x} \mid \varphi(\boldsymbol{x}) = 0 \, \}, \tag{11}$$

where φ is often chosen as the signed distance of $\boldsymbol{x}$ to the closest point on Γ:

$$\varphi(\boldsymbol{x}) = \begin{cases} \operatorname{dist}(\boldsymbol{x}) & \boldsymbol{x} \text{ outside } \Gamma, \\ -\operatorname{dist}(\boldsymbol{x}) & \boldsymbol{x} \text{ inside } \Gamma, \end{cases} \tag{12}$$

so that $|\nabla\varphi| = 1$. Surface properties can in general be computed from φ, e.g. the surface normal can be computed as

$$\boldsymbol{n} = \nabla\varphi/|\nabla\varphi|\,, \tag{13}$$

and the mean curvature is given by the divergence of the normal, thus:

$$\kappa = \nabla\cdot(\nabla\varphi/|\nabla\varphi|)\,. \tag{14}$$

The surface itself is advanced by the following advection equation

$$\frac{\partial\varphi}{\partial t} + \boldsymbol{u}\cdot\nabla\varphi = 0. \tag{15}$$

3 Method

3.1 Particle function approximation

The present work is based on a Lagrangian hybrid particle (level set) method Hieber and Koumoutsakos (2005). Denoting discretized quantities with the superscript h, a vector-valued function $\boldsymbol{c}$ is represented by a superposition of particles as

$$\boldsymbol{c}^h(\boldsymbol{x},t) = \sum_p \boldsymbol{C}_p\,\zeta^h(\boldsymbol{x}-\boldsymbol{x}_p(t)), \tag{16}$$

where the $\boldsymbol{C}_p$ are the particle weights and $\boldsymbol{x}_p$ the particle positions. Given a characteristic discretization spacing h, the particle kernel function $\zeta^h(\boldsymbol{x}) = h^{-d}\,\zeta(\boldsymbol{x}/h)$ is smooth and has the interpolating delta-Kronecker property

$$\zeta(\boldsymbol{k}) = \delta_{\boldsymbol{0}\boldsymbol{k}} \tag{17}$$

at the discrete particle locations $\boldsymbol{x}_p = \boldsymbol{k}\,h$, with $\boldsymbol{k}$ a multi-index in $\mathbb{Z}^d$. Moreover, it satisfies the following moment conditions

$$\int \zeta\,\boldsymbol{x}^\alpha\,d\boldsymbol{x} = \boldsymbol{0}^\alpha \qquad 0\le\alpha<r, \tag{18}$$

where $r>0$ is called the order of the kernel,

The level-set function is approximated according to Eq. (16) as

$$\varphi^h(\boldsymbol{x},t) = \sum_p \varphi_p(t)\,v_p(t)\,\zeta^h(\boldsymbol{x}-\boldsymbol{x}_p(t)), \tag{19}$$

where the v_p represent the particle volumes.

The discretization of Eqs. (5) and (10) using the particle function representation (16) leads to the following system of ordinary differential equations:

$$\begin{aligned}
\frac{d\boldsymbol{x}_p}{dt} &= \boldsymbol{u}(\boldsymbol{x}_p, t),\\
\frac{d\boldsymbol{C}_p}{dt} &= v_p\, \boldsymbol{F}(\boldsymbol{c}) + v_p \underline{\underline{\boldsymbol{D}}} \nabla^h \cdot \left((\mathbb{1} - \boldsymbol{n} \otimes \boldsymbol{n}) \nabla^h \boldsymbol{c} \right),\\
\frac{d\varphi_p}{dt} &= 0,\\
\frac{dv_p}{dt} &= v_p\, \nabla^h \cdot \boldsymbol{u},
\end{aligned} \tag{20}$$

where $\underline{\underline{\boldsymbol{D}}} = \mathrm{diag}(D_1, D_2, \ldots, D_{N_S})$. Using particles initially distributed on regular grid locations $\boldsymbol{x}_p = \boldsymbol{i}\, h$, with $\boldsymbol{i}$ a grid-point index in $\mathbb{Z}^d$, and initial values $v_p = h^d$ and $\boldsymbol{C}_p = h^d\, \boldsymbol{c}(\boldsymbol{x}_p, t = 0)$, the system can be numerically integrated in time.

3.2 Lagrangian distortion and remeshing

As particles follow the flow map $\boldsymbol{u}$, their locations eventually become distorted and need to be regularized to ascertain convergence Koumoutsakos (2005). Regularization is performed by "remeshing" the particles periodically, i.e. resetting particle locations by interpolating the particle quantities onto a regular grid. This regularization in general has to be performed with a period $\Delta t < \|\nabla \otimes \boldsymbol{u}\|_\infty^{-1}$ in order to prevent particle trajectories from crossing. To simplify the level-set computations, however, we remesh at each time step. By virtue of the delta-Kronecker property of the particle kernel ζ^h, this can be performed as a simple function evaluation:

$$\boldsymbol{C}_p^{\mathrm{new}} = h^d \sum_{p'} \boldsymbol{C}_{p'}\, \zeta^h(\boldsymbol{x}_{p'} - \boldsymbol{x}_p^{\mathrm{new}}), \tag{21}$$

where $\boldsymbol{x}_p^{\mathrm{new}} = \boldsymbol{i}\, h$, and $\boldsymbol{i}$ is a grid-point index in $\mathbb{Z}^d$. Due to the moment properties of ζ, total mass is conserved by this operation and, depending on the order of ζ, also higher order moments are conserved.

For the level-set function φ the situation is slightly different: the level set is not subject to a conservation law, but to the non-conservative advection Eq. (15). We therefore remesh the level-set function as:

$$\varphi_p^{\mathrm{new}} = \left(\sum_{p'} h^d \zeta^h(\boldsymbol{x}_{p'} - \boldsymbol{x}_p^{\mathrm{new}}) \right)^{-1} \sum_{p'} v_{p'}\, \varphi_{p'}\, \zeta^h(\boldsymbol{x}_{p'} - \boldsymbol{x}_p^{\mathrm{new}}), \tag{22}$$

thus enforcing partition of unity.

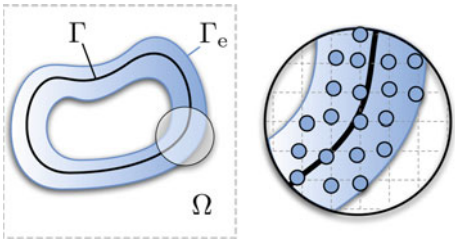

Fig. 1 Extension of the geometry Γ into Ω. Both the level-set function φ and the concentrations c_s are defined in the extended geometry Γ_e

3.3 Level set reinitialization and function extension

As the level set is advected by Eq. (15), it eventually loses its signed-distance property and it needs to be "redistanced" or "reinitialized". The approach we employ in this work is based on Sussman et al. (1994), where the following PDE is evolved in an artificial time τ to steady state:

$$\frac{\partial \varphi}{\partial \tau} - \operatorname{sign}(\varphi_o)\,(1 - |\nabla \varphi|) = 0\,, \tag{23}$$

where $\varphi_o = \varphi(\tau = 0)$. Equation (23) is solved using the scheme formulated in Jiang and Peng (2000).

As we are solving the conservation law formulation (10), we need to extend both the concentrations $\boldsymbol{c}$ and the velocities $\boldsymbol{u}$ off the interface Γ, in a way that satisfies the requirements (9). As we are only interested in the concentrations on Γ, it suffices to extend the quantities into a narrow band around the level set (see Fig. 1), which we define as

$$\Gamma_e = \left\{ \boldsymbol{x} \;\middle|\; |\varphi(\boldsymbol{x})| \leq \gamma \right\}. \tag{24}$$

All calculations are restricted to this narrow band. The narrow-band thickness γ depends on the discretization of spatial operators, and is in general $\gamma < 10h$, where h is the spacing of the discretization. We periodically extend the concentrations by solving the following PDE according to Chen et al. (1997) and Peng et al. (1999):

$$\frac{\partial c_s}{\partial \tau} + \operatorname{sign}(\varphi) \nabla \varphi \cdot \nabla c_s = 0\,, \tag{25}$$

which leads to $\frac{\partial c_s}{\partial n} = 0$. We note that any other redistancing and extension scheme can be used instead, e.g. the Fast Marching Method of Sethian (1999) and Osher and Fedkiw (2003). In general, the same procedure also has to be applied to the velocity $\boldsymbol{u}$. In the case where the velocity only depends on $\boldsymbol{c}$, it suffices, however, to compute $\boldsymbol{u}$ from the extended $\boldsymbol{c}$.

Summarizing, the complete algorithm based on explicit Euler integration of the ordinary differential equations becomes:

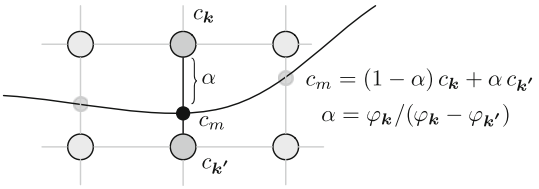

Fig. 2 The intersection point of the interface Γ with the connection of $\boldsymbol{k}$ and $\boldsymbol{k}'$ is calculated using linear interpolation. The function c is evaluated at that point by interpolating the values from $\boldsymbol{k}$ and $\boldsymbol{k}'$

Initialize fields $\boldsymbol{c}$ *and* φ
for $n = 0, \ldots, T$ with time step size δt **do**
Extend $\boldsymbol{c}$ *to the narrow band* $\Gamma_{\mathrm{e}} \to \tilde{\boldsymbol{c}}$
Compute the velocity $\boldsymbol{u}$ *from* $\tilde{\boldsymbol{c}}$ *and* φ.
Create particles from the fields $\tilde{\boldsymbol{c}}$ *and* φ. *Particles have locations* $\boldsymbol{x}_p^n$ *and carry strengths* $\boldsymbol{c}_p^n$ *and* φ_p^n.
Move the particles using the velocity $\boldsymbol{u}$
Interpolate particles back onto the mesh (remeshing)
Compute reaction and diffusion terms on grid locations and update $\boldsymbol{c}^n \to \boldsymbol{c}^{n+1}$
Redistance the level set φ
end for

4 Results

4.1 Accuracy

In order to assess the accuracy of the present calculations we first conduct a refinement study for the approximation of the intrinsic Laplacian on a sphere. We compute the maximum error as

$$E_\Delta = \|\Delta_\Gamma\, c - \nabla^h \cdot \Big((\mathbb{1} - \boldsymbol{n} \otimes \boldsymbol{n})\nabla^h c^h\Big)\|_\infty. \tag{26}$$

The discrete $\|\cdot\|_\infty$-norm above is given by

$$\|c\|_\infty = \max_{\boldsymbol{m} \in \mathcal{M}_\Gamma} |c_{\boldsymbol{m}}|\,, \tag{27}$$

with $\mathcal{M}_\Gamma$ being the set of all points where the connection between two particles/grid points intersects the interface Γ (see Fig. 2). As a function we consider

$$c(\phi, \theta) = Y_1^0(\phi, \theta), \tag{28}$$

where Y_1^0 is the $(1, 0)$ spherical harmonic. The exact solution is given by

$$\Delta_\Gamma c(\phi, \theta) = -2\, Y_1^0(\phi, \theta). \tag{29}$$

Table 1 Maximum error and convergence rate for different resolutions h of the discretized Laplacian on a sphere

h	E_Δ	Conversion rate
1/8	1.13×10^{-2}	–
1/16	3.55×10^{-3}	1.66
1/32	8.48×10^{-4}	2.07
1/64	2.19×10^{-4}	1.96

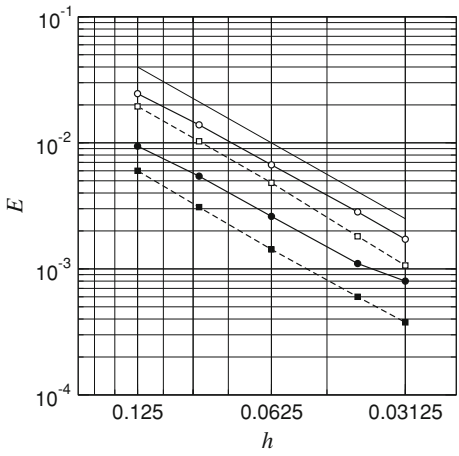

Fig. 3 Refinement study for growth only: L_2 and L_∞ errors at time $T = 0.4$. We plot the errors of concentration—*solid lines with black circles* (L_2) and *white circles* (L_∞)—and interface location—*dashed lines with black squares* (L_2) and *white squares* (L_∞). The *solid line without symbols* denotes the expected slope for second-order convergence

We consider a sphere of radius $R = 1.0$ and four different resolutions: $h = 1/8$, $1/16$, $1/32$, and $1/64$. As expected from the employed second-order discretization, the approximation is second-order accurate (see Table 1).

In order to assess the accuracy of the presented method in the case of deforming geometries we consider a case without reaction nor diffusion. We initialize a concentration c on the sphere and let the sphere grow with velocity $\boldsymbol{u} = \boldsymbol{n}$. The exact solution for this case is given by a simple rescaling of the initial condition, i.e.

$$c(\boldsymbol{x}, t) = \left(\frac{R}{|\boldsymbol{x}(t)|}\right)^2 c(\boldsymbol{x}/|\boldsymbol{x}|, 0).$$

The initial condition is chosen as (28). Figure 3 displays the convergence measurements for this case.

4.2 Reaction–diffusion systems on a sphere

The first system we consider is the linearized Brusselator from Varea et al. (1999):

$$\begin{aligned} \frac{\partial c_1}{\partial t} &= \alpha\, c_1\,(1 - r_1\, {c_2}^2) - c_2\,(1 - r_2\, c_1) + D_1\, \Delta\, c_1, \\ \frac{\partial c_2}{\partial t} &= \beta\, c_2 \left(1 + \frac{\alpha\, r_1}{\beta}\, c_1\, c_2\right) + c_1\,(\gamma - r_2\, c_2) + D_2\, \Delta\, c_2. \end{aligned} \tag{30}$$

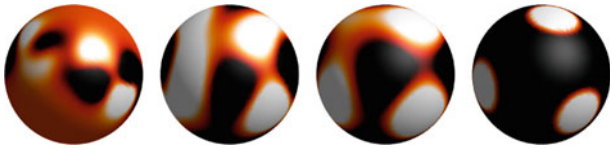

Fig. 4 Simulation of the reaction–diffusion system (30) on the surface of the unit sphere. From left to right: distribution of c_1 after iterations 1,000, 10,000, 100,000, and 200,000

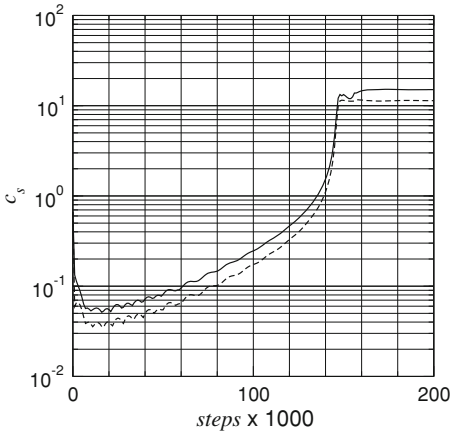

Fig. 5 Evolution of the maxima of $|c_1|$ (*solid line*) and $|c_2|$ (*dashed line*) for the spot-pattern forming system (30) on the unit sphere. The plot illustrates the stiffness of the system and an initial oscillatory phase is apparent during the first 80,000 time steps

We use the same parameters as Varea et al. (1999): $r_1 = 0.02, r_2 = 0.2, D_1 = 0.088, D_2 = 0.516, \alpha = 0.899$, and $\beta = -0.91$. The initial condition is given by $c_1 = c_2 = 0$ except on a band of width 0.2 around the equator, where the values of both c_1 and c_2 are uniformly randomly distributed in $[-0.5, 0.5]$. We obtain the same six-spot pattern as in reference Varea et al. (1999) (see Fig. 4). The evolution of the maxima of c_1 and c_2 are depicted in Fig. 5. The pattern goes through an oscillatory stage in the beginning until the stable steady state is reached after 150,000 time steps.

The second system is an activator-substrate system from Koch and Meinhardt (1994):

$$\begin{aligned} \frac{\partial c_1}{\partial t} &= \rho_1 \frac{{c_1}^2 c_2}{1 + k\,{c_1}^2} - \mu_1\, c_1 + \sigma_1 + D_1\, \Delta_\Gamma\, c_1\,, \\ \frac{\partial c_2}{\partial t} &= -\rho_2 \frac{{c_1}^2 c_2}{1 + k\,{c_1}^2} + \sigma_2 + D_2\, \Delta_\Gamma\, c_2. \end{aligned} \tag{31}$$

For the activator-substrate system (31), we simulate two different parameter sets: $\sigma_1 = 0.0$, $\sigma_2 = 0.02$, $\rho_1 = 0.01$, $\rho_2 = 0.02$, $\mu_1 = 0.01$, $\mu_2 = 0.0$, and $k = 0$ and $k = 0.25$, respectively. The initial condition is given as 10% random perturbations from the steady-state solutions $(1, 1)$ and $(1, 5/4)$ for $k = 0$ and $k = 0.25$, respectively. These parameter choices gave rise to spot patterns and stripe patterns, respectively, on a square lattice in Koch and Meinhardt (1994) and we observe similar patterning on a sphere of radius $R = 0.3$. The results are depicted in Fig. 6 (spots, $k = 0.0$) and Fig. 7 (stripes, $k = 0.25$).

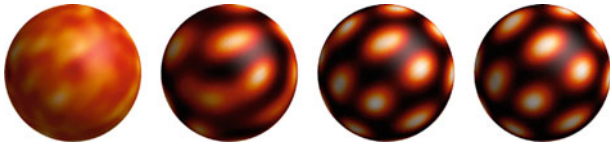

Fig. 6 Simulation of the reaction–diffusion system (31) on a sphere of radius $R = 0.3$ with $k = 0$. From left to right: distribution of c_1 after iterations 1,000, 10,000, 40,000, and 140,000

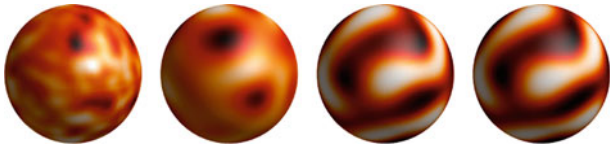

Fig. 7 Simulation of the reaction–diffusion system (31) on a sphere of radius $R = 0.3$ with $k = 0.25$. From left to right: distribution of c_1 after iterations 1,000, 10,000, 40,000, and 140,000

4.3 Reaction–diffusion patterns and growth

A question raised in many studies of developmental systems and organogenesis is: "how is size determined?", e.g., how does an organ know when it has grown large enough? Additionally, how is size related to the scaling of morphogen gradients? In order to illustrate possible studies using the framework presented here, we consider the following simplified system: the initial geometry is a sphere of radius $R = 0.3$ carrying an initial "morphogen" concentration given by

$$c(r, \theta, \phi) = \exp(-16\,\theta^2).$$

This morphogen is subject to diffusion and natural decay, thus:

$$\frac{\partial c}{\partial t} = -\mu\, c + D\, \Delta_\Gamma\, c \tag{32}$$

and causes the geometry to grow with velocity

$$\boldsymbol{u} = \begin{cases} c\,\boldsymbol{n}, & c > 0.01 \\ 0.0, & \text{otherwise.} \end{cases} \tag{33}$$

We measure the "size" of the geometry as the maximum edge length of the bounding box (thus the initial size is 0.6) with time. We consider five different cases with varying morphogen decay rates and diffusivities as listed in Table 2.

As depicted in Fig. 8, the different dynamics of the morphogen lead to distinguishably different dynamics and different final geometries. Increasing the decay rate of the morphogen, e.g., leads to smaller geometries with more localized features, while increasing the diffusivity acts in a way of an implicit surface tension and regularizes the shape.

Table 2 List of the simulation cases considered for system (32)

Case	μ	D
a	2	0.0
b	2	0.01
c	2	0.001
d	$\sqrt{2}$	0.001
e	0.1	0.001

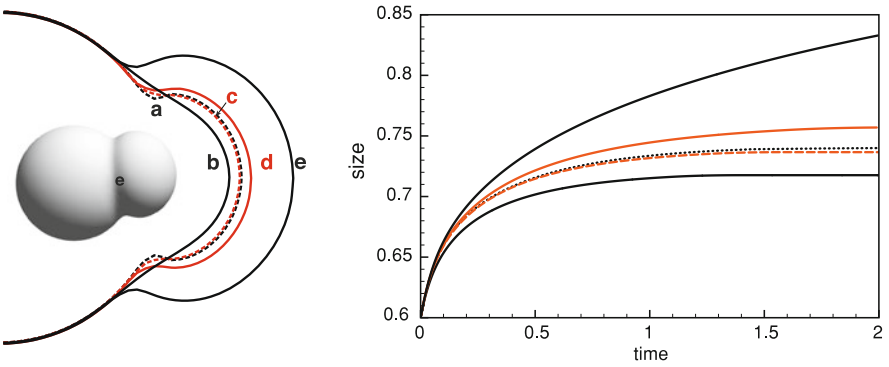

Fig. 8 Crosscuts through the geometry of the growth cases a–e, and 3D rendering of the geometry e in the middle. We simulate growths with varying morphogen diffusion: case a ($D = 0$), b ($D = 0.01$), and c ($D = 0.001$) and decay rates of the morphogen: case c ($\mu = 2$), d ($\mu = \sqrt{2}$), and e ($\mu = 0.1$). The time evolution of the largest extent of the bounding box of the growing geometry is shown in the plot on the right, illustrating the different growth dynamics

We now couple the deformation of the geometry to pattern-forming reaction–diffusion systems by setting the local velocity to

$$\boldsymbol{u} = \boldsymbol{n}\, f(\boldsymbol{c}). \tag{34}$$

We first consider system (31) with $f(\boldsymbol{c}) = c_1$, which always results in an outward motion of the geometry since $c_1 \geq 0$, and thus leads to an increase in surface area. This increase in surface area can be viewed as lowering the effective diffusion constants in the reaction–diffusion system. Since the reactions are generally independent of the surface properties, the only direct effect that growth has on the reaction–diffusion dynamics is the decrease in concentration in the sense of a decay term that depends on the growth velocity. Figure 9 shows the time evolution of this simulated stripe-forming growth system.

As a final example we consider the Gray-Scott multiplying spots pattern (Pearson 1993) on the sphere with $f(\boldsymbol{c}) = \max_\Gamma(c_1) - c_1$. As shown in Fig. 10, the bifurcating nature of the patterning system can to some extent also be identified in the grown geometry.

The growth velocity can also involve more complex properties of the surface. As an example we consider a spot-forming reaction–diffusion system on a dumbbell shape that shrinks under its own curvature, i.e. $\boldsymbol{u} = -\boldsymbol{n}\,\kappa$, where κ is the mean curvature.

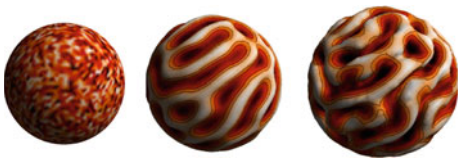

Fig. 9 Growth of the stripe pattern of system (31) at iterations 0, 50,000, and 80,000

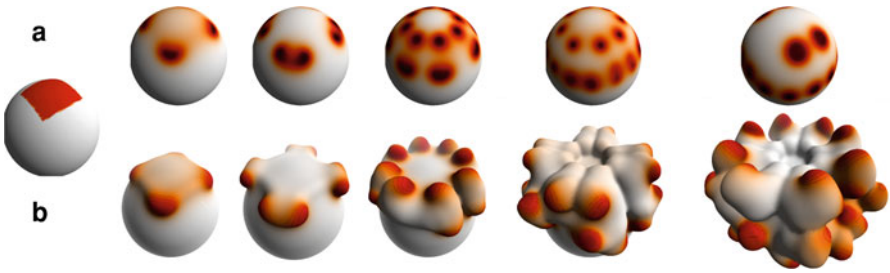

Fig. 10 Growth proportional to the concentration of a morphogen governed by the Gray–Scott reaction–diffusion system for the initial condition shown on the very left. Surfaces from left to right represent the evolution of the system without growth (a) and with growth (b) at iterations $800 \times j$, for $j = 0, 1, 2, 4, 6, 8$. The *colors* represent the concentration of c_1 with *red* indicating high concentrations and *light gray* low concentrations

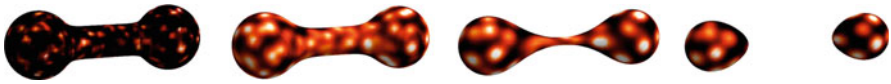

Fig. 11 Spot pattern generated by solving Eq. (31) on a dumbbell shrinking under mean curvature flow. This also illustrates the robustness of the present method with respect to certain topological changes, including fission of an object

The curvature is a local property of the geometry and is computed from the level set through Eq. (14). The evolution of the geometry is depicted in Fig. 11 and illustrates the robustness of the present method with respect to topological changes involving break-up of interfaces. This robustness is directly inherited from the underlying level-set formalism. Obtaining correct behavior in cases of fusion of two geometries, however, requires some care in the computation of surface properties (Macklin and Lowengrub 2005).

5 Conclusion

We have developed a novel particle method for the simulation of reaction–diffusion processes on complex deforming surfaces. In this method, particles are used to discretize the geometry of the surface by approximating its suitable implicit level-set representation. The initial geometry can be analytically given or reconstructed from 3D imaging data, as has been done for the endoplasmic reticulum in live cells by Sbalzarini et al. (2006). Surface differential operators are embedded in the level-set representation and discretized on the same set of Lagrangian particles. This unifying particle representation of the geometry and the reaction–diffusion dynamics enables

simulations of high accuracy, and can carry out reaction–diffusion simulations even in cases where surfaces are dynamically disconnected. We note, however, that at the moment of disconnection the validity of the underlying continuum model is questionable and multiscale models, coupling microscopic events to the continuum description, are necessary.

The proposed method has been validated on benchmark problems with analytical solutions and its capabilities have been demonstrated on surfaces evolving under morphogen distributions and/or curvature. Current work involves applications of these techniques to problems of developmental biology, and extending models of tumor-induced angiogenesis (Milde et al. 2008). Furthermore we consider the integration of cellular and molecular models as dictated by the need to provide a "closure" for the continuum models when considering the merging and separation of surfaces corresponding to biological systems.

Acknowledgments We thank the reviewers of this manuscript for their constructive comments. The authors are greatful to support from the Swiss SystemsX.ch initiative and from the Swiss National Science Foundation.

References

Adalsteinsson D, Sethian JA (2003) Transport and diffusion of material quantities on propagating interfaces via level set methods. J Comput Phys 185:271–288

Baker R, Maini P (2007) A mechanism for morphogen-controlled domain growth. J Math Biol 54(5):597–622

Bänsch E, Morin P, Nochetto RH (2005) A finite element method for surface diffusion: the parametric case. J Comput Phys 203:321–343

Bergdorf M, Koumoutsakos P (2006) A Lagrangian particle-wavelet method. Multiscale Model Simul 5(3):980–995

Bertalmio M, Cheng L-T, Osher S, Sapiro G (2001) Variational problems and partial differential equations on implicit surfaces. J Comput Phys 174:759–780

Chaplain MAJ, Ganesh M, Graham IG (2001) Spatio-temporal pattern formation on spherical surfaces: numerical simulation and application to solid tumour growth. J Math Biol V42(5):387–423

Chen S, Merriman B, Osher S, Smereka P (1997) A simple level set method for solving Stefan problems. J Comput Phys 135:8–29

Enright D, Fedkiw R, Ferziger J, Mitchell I (2002) A hybrid particle level set method for improved interface capturing. J Comput Phys 183(1):83–116

Harrison LG, Kolar M (1988) Coupling between reaction–diffusion prepattern and expressed morphogenesis, applied to desmids and dasyclads. J Theor Biol 130(4):493–515

Harrison LG, Wehner S, Holloway DM (2001) Complex morphogenesis of surfaces: theory and experiment on coupling of reaction–diffusion patterning to growth. Faraday Discuss 120:277–294

Hieber SE, Koumoutsakos P (2005) A Lagrangian particle level set method. J Comput Phys 210(1):342–367

Holloway DM, Harrison LG (1999) Algal morphogenesis: modelling interspecific variation in Micrasterias with reaction–diffusion patterned catalysis of cell surface growth. Phil Trans R Soc Lond B 354:417–433

Jiang G-S, Peng D (2000) Weighted ENO schemes for Hamilton–Jacobi equations. SIAM J Sci Comput 21(6):2126–2143

Kaandorp JA, Sloot PMA, Merks RMH, Bak RPM, Vermeij MJA, Maier C (2005) Morphogenesis of the branching reef coral *madracis mirabilis*. Proc R Soc B 272:127–133

Koch AJ, Meinhardt H (1994) Biological pattern formation: from basic mechanisms to complex structures. Rev Modern Phys 66(4):1481–1507

Koumoutsakos P (2005) Multiscale flow simulations using particles. Annu Rev Fluid Mech 37(1):457–487

Macklin P, Lowengrub J (2005) Evolving interfaces via gradients of geometry-dependent interior poisson problems: application to tumor growth. J Comput Phys 203:191–220
Macklin P, McDougall S, Anderson A, Chaplain M, Cristini V, Lowengrub J (2009) Multiscale modelling and nonlinear simulation of vascular tumour growth. J Math Biol 58(4):765–798
Madzvamuse A, Maini PK (2007) Velocity-induced numerical solutions of reaction–diffusion systems on continuously growing domains. J Comput Phys 225:100–119
Milde F, Bergdorf M, Koumoutsakos P (2008) A hybrid model for three-dimensional simulations of sprouting angiogenesis. Biophys J 95(7):3146–3160
Murray JD (2002) Mathematical biology I: an introduction. In: Interdisciplinary applied mathematics, vol 17. Springer, New York
Osher S, Fedkiw R (2003) Level set methods and dynamic implicit surfaces. In: Applied mathematical sciences, vol 153. Springer, New York
Pearson JE (1993) Complex patterns in a simple system. Science 261(5118):189–192
Peng D, Merriman B, Osher S, Zhao H, Kang M (1999) A PDE-based fast local level set method. J Comput Phys 155:410–438
Ruuth SJ, Merriman B (2008) A simple embedding method for solving partial differential equations on surfaces. J Comput Phys 227(3):1943–1961
Sbalzarini IF, Hayer A, Helenius A, Koumoutsakos P (2006) Simulations of (an)isotropic diffusion on curved biological surfaces. Biophys J 90(3):878–885
Sethian JA (1999) Fast marching methods. SIAM Rev 41(2):199–235
Stone HA (1990) A simple derivation of the time-dependent convective-diffusion equation for surfactant transport along a deforming interface. Phys Fluids A 2(1):111–112
Sussman M, Smereka P, Osher S (1994) A level set approach for computing solutions to incompressible two-phase flow. J Comput Phys 114(1):146–159
Thompson DW (1942) On growth and form, 2nd edn. Cambridge University Press, Cambridge
Turing AM (1952) The chemical basis of morphogenesis. Philos Trans R Soc Lond Ser B 237(1/2):37–72
Varea C, Aragon JL, Barrio RA (1999) Turing patterns on a sphere. Phys Rev E 60(4):4588–4592
Xu J-J, Zhao H (2003) An eulerian formulation for solving partial differential equations along a moving interface. SIAM J Sci Comput 19(1–3):573–594